



HAL
open science

Immobilization of TiO₂ nanoparticles on natural *Luffa cylindrica* fibers for photocatalytic applications

Mohamad El-Roz, Zeinab Haidar, Louwanda Lakiss, Joumana Toufaily,
Frederic Thibault-Starzyk

► To cite this version:

Mohamad El-Roz, Zeinab Haidar, Louwanda Lakiss, Joumana Toufaily, Frederic Thibault-Starzyk. Immobilization of TiO₂ nanoparticles on natural *Luffa cylindrica* fibers for photocatalytic applications. RSC Advances, 2013, 3 (10), pp.3438-3445. 10.1039/c2ra22438k . hal-01963800

HAL Id: hal-01963800

<https://hal.science/hal-01963800v1>

Submitted on 10 Nov 2021

HAL is a multi-disciplinary open access archive for the deposit and dissemination of scientific research documents, whether they are published or not. The documents may come from teaching and research institutions in France or abroad, or from public or private research centers.

L'archive ouverte pluridisciplinaire **HAL**, est destinée au dépôt et à la diffusion de documents scientifiques de niveau recherche, publiés ou non, émanant des établissements d'enseignement et de recherche français ou étrangers, des laboratoires publics ou privés.

Cite this: DOI: 10.1039/c0xx00000x

www.rsc.org/xxxxxx

ARTICLE TYPE

Immobilization of TiO₂ nanoparticles on natural *Luffa cylindrica* fibers for photocatalytic applications

Mohamad El-Roz,^{*a} Zeinab Haidar,^{a,b} Louwanda Lakiss,^a Joumana Toufaily,^{b,c} Frederic Thibault-Starzyk^a

Received (in XXX, XXX) Xth XXXXXXXXXX 20XX, Accepted Xth XXXXXXXXXX 20XX

DOI: 10.1039/b000000x

TiO₂/Luffa composites have been successfully prepared via a sol-gel method from the hydrolysis of a precursor of TiO₂. The possibility to use Luffa fibers as biotemplate to self-support hierarchical TiO₂ macrostructures has been also tested with success. The photocatalysts used or prepared and the TiO₂/Luffa composites were characterized by X-ray diffraction, scanning electron microscopy, thermal gravimetric analysis, FT-IR, and UV-visible spectroscopy. The photocatalytic activities have been investigated in the photodegradation of methanol, chosen as model molecules for VOCs in air. The reactions have been followed by IR-operando spectroscopy. TiO₂/Luffa composites exhibited a good stability and photocatalytic activity under UV light irradiation, giving rise to a new generation of green photocatalysts, easy to shape and manufacture, for the photodegradation of organic pollutants.

1. Introduction

In the last few years TiO₂ has attracted much more attention due to its interesting properties as a semi-conductor: it is cheap, non toxic, photostable, resistant to photocorrosion and presents high photocatalytic activity to decompose a wide type of hazardous organic compounds that are present in air or water. Because of these notable characteristics, TiO₂ is the most well-known and frequently used catalyst in photocatalysis. Moreover, titanium dioxide nanostructures are also promising materials for various applications including photoelectronic, solar energy conversion, self-cleaning surfaces, etc.

Although titanium dioxide is an ideal environmental photocatalyst, it has some drawbacks that limit its large-scale application especially when it is used in the nanosized form. For instance, the removal and recycling of the photocatalyst after the reaction process are very difficult. In addition titanium dioxide nanostructures dispersed in the reaction media could be hazardous, due to their potential inflammatory and cytotoxic effects [1]. In this context, immobilization of the photocatalysis on a specific support could be of great benefit. Several attempts have been already reported in the literature [2–22] and various techniques were successfully used to immobilize TiO₂ on different supporting materials such as SiO₂ glass beads [2], rings [3], and reactor tubular walls [4,5]; fiber-glass [6,7]; quartz [8,9]; zeolites [10,11]; perlite [12]; pumice [13]; alumina-based ceramic [14]; stainless steel [15,16]; aluminum [17]; polymeric membranes [18–20]; etc.

Natural fibers were also found of great interest as supporting materials, and cotton conveniently adapted inside the photoreactors [21–23]. These fibers are inexpensive, abundant, environmentally benign and renewable resources. Recently we have used Luffa sponge (aegyptica or cylindrica) to support free-organic template zeolite materials, with high efficiency. It is a tropical annual climber vine plant (family Cucurbitaceae), with fruits possessing a net-like fibrous vascular system (Luffa sponges). The struts of this natural sponge are characterized by microcellular architecture with continuous hollow microchannels (macropores with diameter of 10–20 μm) which allow a good supporting of inorganic materials (Fig. 1). The network of the Luffa fibers provides a tridimensional form for the support that allows a good penetration of the light and decreases the density of the fibers. Besides, the fibers nature makes the shaping of filters in different geometry and form easier. In addition, these fibers present a high stability in the synthesis media and support the relatively high temperature (<170°C) and alkalinity of the synthesis media. Luffa sponges have also been applied as cell carriers in bioreactors [24], scaffolds for tissue engineering [25], for the development of biofiber-reinforced composites [26] and as biotemplate to self-support hierarchical zeolite macrostructures for bio-inspired structured catalytic reactors [27].

Since researches on immobilized TiO₂ photocatalysts were mostly focused on the use of the commercial TiO₂ P25 or anatase phase, we focused on supporting TiO₂ anatase nanoparticles, by sol-gel method, on Luffa sponges as natural supports. The possibility to use Luffa fibers as biotemplate to self-support hierarchical TiO₂ macrostructures will also be presented in this paper. The resulting TiO₂/Luffa composite has been fully characterized and

investigated as photocatalyst for the degradation of methanol as model molecule for VOCs in air.

2. Experimental part

2.1. Synthesis

2.1.1. Chemical treatment of *Luffa* fibers

Luffa fibers were obtained from a local specialty shop. They were washed with acetone in an ultrasonic bath at room temperature for 7 minutes. The fibers were then rinsed with water and dried at 60°C. After drying, the fibers were then treated in a sodium hydroxide solution (NaOH, 0.1M) at 80°C for 2 h. This treatment was done three times, in order to activate the cellulose fibers and remove the other constituents present between the fibers. After each step the fibers were filtered and washed with distilled water until reaching neutral pH.

2.1.2. Synthesis of TiO₂ photocatalysts supported on *Luffa* fibers

TiO₂ nanocrystals were prepared via a sol-gel process followed by hydrothermal treatment. Titanium (IV)-Etoxide (Ti(OEt)₄, TTE 33% Alpha Aesar) was used as titanium source for the preparation of TiO₂ photocatalysts. Absolute ethanol (99%) was used as solvent. The temperature and synthesis time were optimized prior to the preparation of the composites. In a typical procedure, the reaction was carried out with the following composition: 10 TTE/ 45 C₂H₅OH/ 45 H₂O vol.%. The treated fibers were first dispersed in a mixture of water and ethanol (50/50 vol.%; 90 ml). Then TTE has been added drop-wise to the treated fibers (m~500 mg) under vigorous stirring at ambient temperature. A white suspension was obtained. The resulting mixture (suspension + *Luffa*) was kept under stirring for 1 h. Then, the mixture was transferred in a Teflon-lined stainless steel autoclave and heated at different temperature (60-100 °C) from 1 to 48 h. After cooling down to room temperature, the TiO₂/*Luffa* fibers were washed for 5-10 minutes in an ultrasonic bath in order to remove the weakly suspended particles. In order to show the possibility to use the *Luffa* support as biotemplate for hierarchical TiO₂ synthesis, a calcination of TiO₂/*Luffa* composite has been performed at 500°C for 6h under air at atmospheric pressure.

2.2. Characterization

TiO₂ and TiO₂/*Luffa* composites were characterized by X-ray diffraction (XRD; PANanalytical (X-Pert Pro) diffractometer with CuKα1 source (λ=0.15406 nm, 40 kV, 30 mA)), thermal gravimetric analysis (SETARAM), Scanning Electron Microscope (SEM, Phillips CM 20) operating at 200kV), Nitrogen sorption measurements (Micromeritics ASAP 2020 micropore analyser) and by UV-Vis DR measurements (Thermo-electron evolution 500 UV-Vis spectrometer equipped with RSA-CU40 Diffuse Reflectance cell).

2.3. Photocatalytic application

The photocatalytic oxidation of methanol was followed by IR spectroscopy of the solid surface (IR-operando) and of the gas phase. TiO₂/*Luffa* composites were pressed into self-supported wafers (Ø= 16 mm, m~40 mg/cm²) (Fig. 1-c). IR spectra were collected with a Nicolet 5700 FT-IR spectrometer (64 scans/spectrum) equipped with a MCT detector. The operando system was connected to a flow set-up. Gases were introduced into the lines (heated at 60°C) by mass flow controllers. The two gas mixtures, so called “activation” and “reaction” flows, could be prepared and sent independently to the reactor cell. The “Sandwich” reactor-cell used in this study is an evolution of the *operando* cell which has proven its reliability over many years of *operando* studies.[29-31] It was made of a stainless steel cylinder that carries a toroidal sample holder in its centre, where the catalyst self supporting wafer was placed. Tightness was obtained by Kalrez® O-rings, and the dead volume (typically defined as the residual space between each sample face and the windows) was reduced to about 0.4 ml by filling the empty space with KBr windows placed on each side of the sample holder. Analysis of the surface was made possible without superposition of the gas phase signal and fluid dynamics was similar to that inside a honeycomb monolith. Gases were introduced on the sample by 1/8" OD pipe and collected on the opposite side of the sample holder. More details can be found in the following references [29,31]. For this specific photocatalytic oxidation study, UV irradiation was carried out with a polychromatic light of a Xe-Hg lamp (LC8 spot light Hamamatsu, L10852, 200 W), by using a UV-light guide (A10014-50-0110) mounted at the entrance of a modified IR operando cell (Scheme S-1 in supporting information) in order to establish a “homogeneous” irradiation. The intensity of the lamp was about 15 mW/cm² at λ=365 nm for a full irradiation capacity (100%) of the LC8 unit. It was difficult to calculate the intensity of the polychromatic irradiation. Therefore, the intensity values were presented in (%) of the lamp capacity.

In such a configuration, at atmospheric pressure, a low partial pressure of VOC was established using a saturator at a carefully controlled temperature. The gas mixture composition was then fixed at 0.01 to 0.2 vol.% methanol, 20 vol.% O₂ in Ar and the total flow was adjusted to 25 cm³/min. Analysis of the outlet gases was performed by means of a Nicolet 5700 FT-IR-gas spectrometer using a gas microcell.

The photooxidation of methylene blue in water was also performed on TiO₂/*Luffa* composite to show efficiency in dye removal. Due to high absorption/adsorption capacity, photooxidation tests have been realized after absorption by using *Luffa* fibers as reference and the results of this part were reported in supplementary information. The photocatalytic activity was qualitatively estimated based on the color of the composites and of the *Luffa* fibers after irradiation.

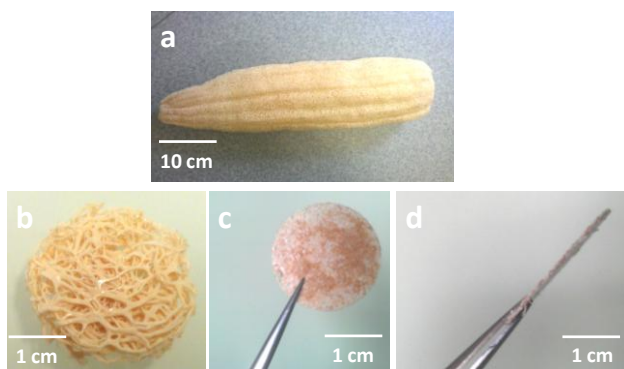


Fig.1 Image of Luffa fruit (a) and TiO₂/ Luffa composites (b-d): Face (c) and side (d) view of the pellet.

3. Results and discussion

3.1. Characterization of TiO₂/Luffa composites

Prior to the preparation of the TiO₂/Luffa composites, the sol-gel synthesis conditions of TiO₂ have been first optimized. Two parameters were considered: the synthesis time and the temperature. For further details, readers are invited to see the supporting information file. The synthesis of the TiO₂/Luffa composites has been performed at 100 °C for 48 hours. The X-ray diffraction pattern of the resulting TiO₂/Luffa composite is reported in Fig. 2. It shows in addition to the Bragg reflexions of the cellulose (L), the main constituent of the fibers, the Bragg reflections of the anatase TiO₂ phase (A). For comparison, the X-ray diffraction pattern of the anatase phase and the plain Luffa fibers are also reported in this figure. The powder that has been recovered from the bottom of the autoclave after synthesis was also characterized by XRD. It shows the Bragg reflections of the anatase type phase. Such a result confirms the high crystallinity

and purity of the composites prepared.

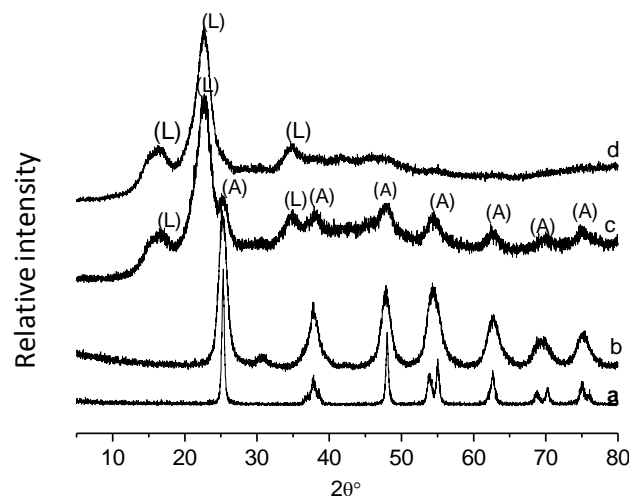


Fig.2 X-ray diffraction patterns for TiO₂ samples (a) standard, (b) TiO₂ powder recovered after the synthesis, (c) TiO₂ deposited on Luffa fibers (d) Luffa fibers.

Fig. 3 shows the SEM images of the plain Luffa fibers (a-c) and TiO₂/Luffa composite after ultrasonic treatment (d-f). As seen in this figure, the microfibrils structure is completely preserved after the hydrothermal treatment and TiO₂ nanoparticles are uniformly dispersed and grown on and through the Luffa fibers. The fibers are completely covered and the radius of the TiO₂ nanoparticles is about 15-20 nm. Indeed, the net microstructures and hydroxyl groups of the Luffa fibers provided a homogeneous dispersion of TiO₂ nanoparticles, as well as a strong and complete recovery of the surface. Hydroxyl groups of cellulose may play a key role in the synthesis and growth of TiO₂ nanoparticles by condensation reaction ($\text{TiOH} + \text{HOC} \rightarrow \text{TiOC} + \text{H}_2\text{O}$) and/or by hydrogen bonding.

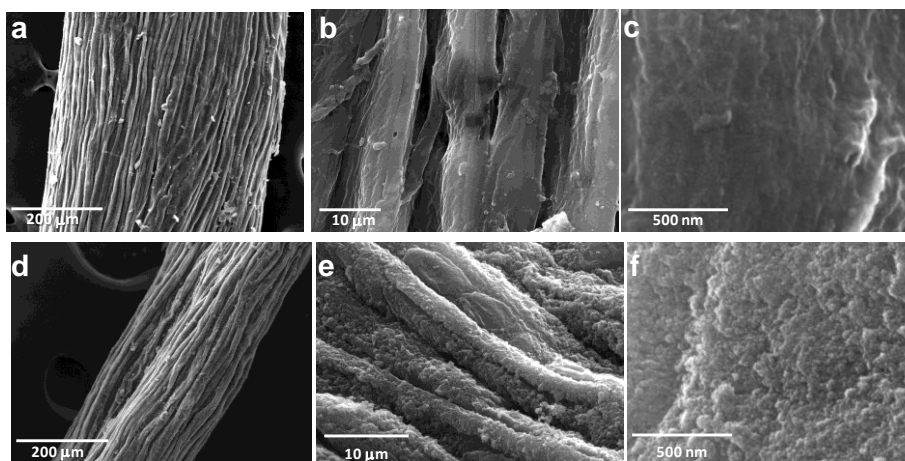


Fig.3 SEM pictures of treated Luffa fibers before (a-c) and after TiO₂ deposition (d-f).

In order to investigate the thermal stability and estimate the amount of TiO₂ recovery for the composites, thermal analyses have been performed. The samples were heated from 25 to 800 °C with a heating rate of 5 °C/min. Fig. 4 shows the thermogravimetric curves of pure TiO₂ (a), TiO₂/Luffa composite (b) and plain Luffa (c) samples. For pure TiO₂ sample, one main weight loss of about ~8% appeared above 150 °C. This could be assigned to the desorption of water adsorbed on TiO₂ surface. An additional small weight loss occurred progressively above 150 °C (insert of Fig. 4). This later could be ascribed to the dehydroxylation of TiOH groups at high temperature (150-400°C). The thermogravimetric curves of the plain Luffa fibers and TiO₂/Luffa composites showed the same behaviour. Both were stable for below 250 °C. A weight loss appeared above this temperature, assigned to the degradation of the organic constituents of the fibers. The total weight loss observed for plain Luffa fibers was about 97.5 %. The residual 2.5 % of the weight corresponded to mineral compounds present in the fibers. For TiO₂/Luffa composite, the total weight loss observed was ~93.9%. Based on the results obtained for plain Luffa fibers, the amount of TiO₂ deposited could be estimated to ~4% (TiO₂ (%) = 97.5-93.9=3.6%). It is noteworthy that the amount of water desorbed below 150°C was more pronounced for plain Luffa fibers than for the TiO₂/Luffa sample. Such a result demonstrates that the plain Luffa fibers are more hydrophilic than the composites, which explains the high adsorption/absorption capacity of methylene blue by TiO₂/Luffa (Fig. S.3, supplementary information). The reproducibility of this result has also been tested using different samples synthesized under the same conditions. The error on the TiO₂ amount was estimated below 2%.

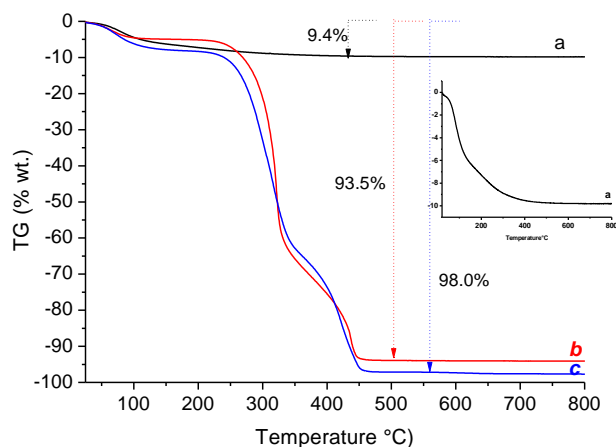


Fig.4 Thermogravimetric curves of: (a) as-synthesized TiO₂, (b) TiO₂/Luffa and (c) Luffa. Insert: full scale of the thermogravimetric curves as-synthesized TiO₂.

The effect of temperature on TiOH groups has also been studied by in-situ IR spectroscopy. Fig.5 reports the IR spectra of the as-synthesized TiO₂ sample under air and vacuum at different temperatures. For a temperature higher than 100 °C, a total disappearance of the band assigned to adsorbed water on TiO₂ surface at 1625 cm⁻¹ has been observed. The broad band located at 3160 cm⁻¹ also decreased. We assigned it to hydrogen bonding between neighbouring TiOH groups and/or to water adsorbed on TiOH groups. This decrease was due to water desorption for

T < 100°C and to TiOH dehydroxylation for a higher temperature (TiOH → HOTi → TiOTi + H₂O). These results are in a good agreement with the ATG results discussed above. The narrow bands at ~3720 and ~3670 cm⁻¹ are assigned to Ti(III)OH and Ti(IV)OH bands respectively [29]. When the temperature increased (for 100°C < T < 200°C), the intensity of the band at 3670 cm⁻¹ decreased. This was accompanied by a low increase of the intensity of the band at 3720 cm⁻¹. This could be assigned to a reversible reduction of Ti(IV)OH group by adsorbed water at high temperature.

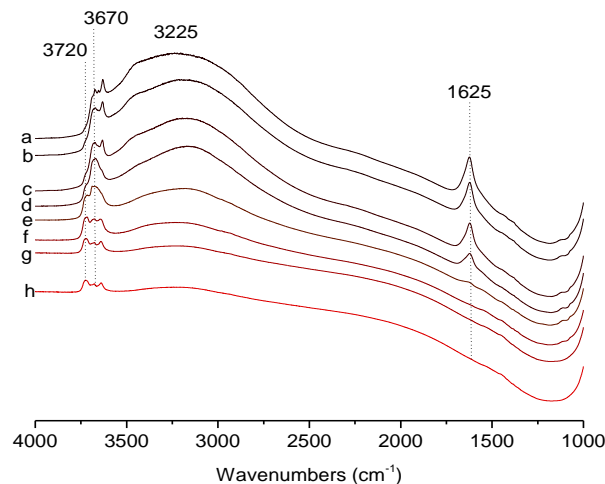


Fig.5 IR spectra of as-synthesized TiO₂ at RT under air (a) and under vacuum (b-h) at RT 50°C (b), 75°C (d), 125°C (e), 200°C (f), 300°C (g) and 350°C (h).

In order to investigate the possibility of using Luffa fibers as biotemplate, a total combustion of the TiO₂/Luffa composite was performed at 500 °C for 6 hours under air. The SEM pictures of the calcined TiO₂/Luffa composite show the formation of a negative replica of TiO₂ macro- microfibers Luffa sponge (TiO₂-L) (Fig. 6). The replica resulted from TiO₂/Luffa calcination confirms the high dispersion and uniform growth of TiO₂ on the Luffa fibers. Moreover, it demonstrates the possibility to use Luffa fibers as a biotemplate to self-support hierarchical TiO₂ macrostructures. According to the XRD results, the negative replica TiO₂-L is a pure anatase. It is noteworthy that the size of the resulting TiO₂ particles significantly increased in comparison with TiO₂/Luffa due to the aggregation of the particles during the calcination.

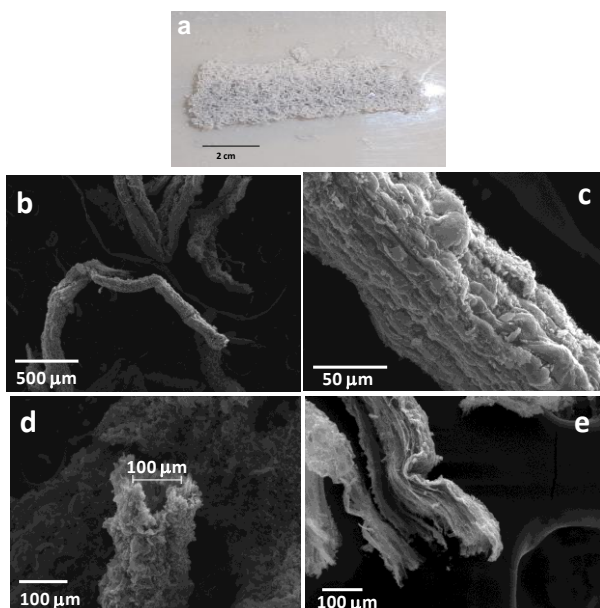


Fig.6 Image (a) and SEM pictures of replica TiO₂ Luffa sponges (TiO₂-L) (b-e).

The TiO₂/Luffa composites and TiO₂-L were also characterized by nitrogen sorption. For comparison, the TiO₂ powder prepared under the same conditions and plain Luffa fibers were also characterized (Fig.7). The porous volume and the specific surface area are reported in table S-1 (see SI). The TiO₂-L and the TiO₂ powder sample both display a type IV isotherm with hysteresis at relatively high pressure. The specific surface area of the TiO₂/Luffa composites is about 16 m²/g while that of TiO₂ powder synthesized under the same condition is 235 m²/g. The specific surface area of the plain Luffa fibres has been found lower than 1 m²/g (Table S-1). Such a result demonstrates that the 16 m²/g founded for TiO₂/Luffa composite is related to the surface area of the microporous TiO₂ particles immobilized on the Luffa. Taking into account the content of TiO₂ in TiO₂/Luffa composite (~4%; see TG results), the specific surface area of TiO₂ supported on the Luffa fibres could be estimated to 400 m²/g (=16/0.04 m²/g). It is much higher than that of unsupported and as-synthesized TiO₂ samples. Such a result confirms the high dispersion of TiO₂ particles on the Luffa fibres. It should be noted that several TiO₂/Luffa samples have been prepared and characterized by nitrogen sorption to test the reproducibility. The results are similar and the error is estimated to ~3%. For TiO₂-L, a significant decrease of the surface area could be observed in comparison with the as-synthesized TiO₂. This decrease is explained by the agglomeration of TiO₂ nanoparticles after calcination.

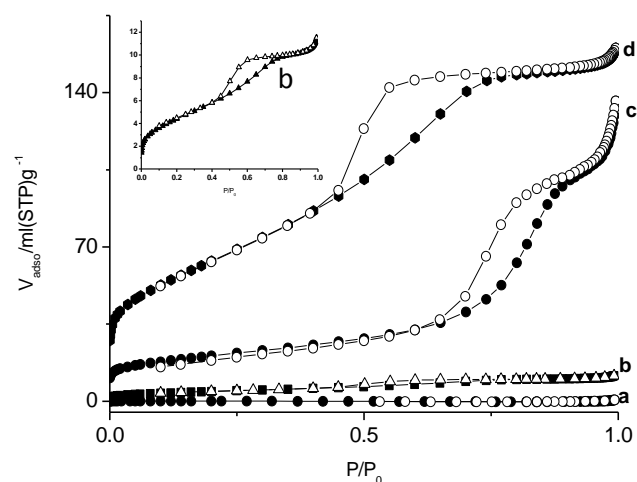


Fig.7 Nitrogen sorption isotherms adsorption (close symbols) and desorption (open symbols) at 77 K for : (a) Luffa fibers, (b) TiO₂/luffa composites, (c) TiO₂-L and (d) TiO₂ powder (the TiO₂ powder recovered after the synthesis).

It is difficult to investigate the UV-visible absorption of TiO₂/Luffa samples due to the low amount of supported TiO₂. For this reason the UV-visible studies were only performed on TiO₂ powder samples (TiO₂-P25, TiO₂ pure anatase and TiO₂-L). The results are reported in Fig.8. It shows that the absorption edge occurs below 405, 416, and 380 nm for TiO₂-P25, TiO₂-L and TiO₂ anatase respectively. The band gap energy is calculated as follows:

Band Gap Energy (E) = $h \cdot C / \lambda$, where h is the Plank constant (6.626×10^{-34} J. s),

C is the speed of light (3.0×10^8 m/s) and λ is the absorption edge wavelength.

As a result the band gap energy (E_g) is found to be equal to 2.99 eV for TiO₂-L, 3.07 eV for TiO₂-P25 and 3.22 eV for TiO₂ pure anatase. Indeed, TiO₂ P25 is a mixture of 80% anatase and 20% rutile. This explains the low E_g compared to TiO₂-anatase. On the other hand, TiO₂-L is a pure anatase as confirmed by XRD, which is contradictory with the E_g found. This result could be assigned to more defects in the TiO₂ structure (Ti(III), TiOH...) than for samples prepared without fibres.

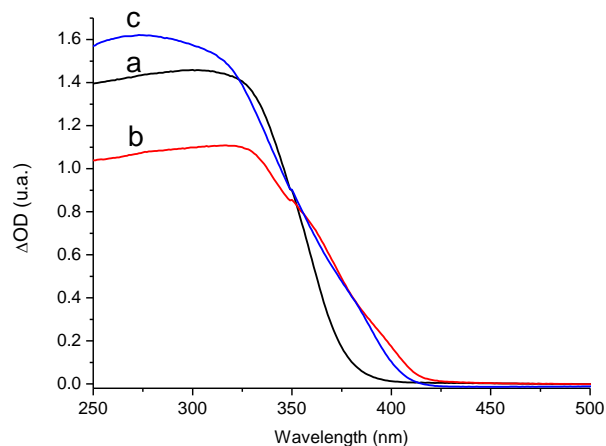


Fig.8 UV-vis spectra of (a) TiO₂-P25, (b) TiO₂-L and (c) TiO₂-anatase.

3.2. photocatalytic applications

The newly elaborated TiO₂/Luffa composites have first been tested in water purification. Methylene blue was used as a model molecule for dyes in water (see experimental part). Due to the different possible pathways of MB photodegradation (direct photolysis and/or photodegradation on TiO₂ surface) [32] and to the difficulty to have a quantitative study for the photoactivity of the composites in water, the results for water purification were shown as a preliminary qualitative analysis in the supplementary information part. The reason to include this part is to highlight the high capacity of the TiO₂/Luffa composite in the removal of dyes from water as show in Fig. S.3. The irradiation of the filter recovered after purification shows an important color modification of the TiO₂/Luffa composite from dark blue to light green which is not the case for plain Luffa fibers (Fig.S.4). The photocatalytic activity of the replica TiO₂-L samples has been also investigated and the results will be discussed in a separate paper.

Herein we will discuss the photocatalytic activity of the TiO₂/Luffa composite in the photodegradation of methanol as a model molecule for volatile organic compounds (VOCs) in air. The photocatalytic degradation of methanol has been carried out under operando conditions.

Fig. 9 presents the evolution of IR spectra of TiO₂/Luffa surface during methanol photooxidation. It is impossible to follow the evolution of CH vibration band due to the saturation of the intensity in this region. As shown in this figure, only the band situated at 5370-4920 cm⁻¹, assigned to (ν+δ) H₂O vibration mode disappears after irradiation. No modification of the bands between 5000 and 3200 cm⁻¹ is observed. In addition a low amount of CO₂ is detected in the first few minutes of irradiation under dry air. This amount is assigned to the degradation of impurities adsorbed on TiO₂/Luffa surface. These results show the high stability of the support under irradiation.

Methanol quantification has been performed from the IR spectra of the gas phase (Fig. 10) using the area of the band at 1090-950 cm⁻¹ assigned to the ν(C-O) vibration mode of methanol. Methanol conversion has been estimated with the following formula:

$$\text{Conversion (\%)} = (A_0 - A_t) / A_0 * 100$$

with:

A₀= the band area of MeOH (in the gas phase) before photooxidation.

A_t= the band area of MeOH during photooxidation at time "t".

The selectivity of MeOH transformation to CO₂ has been calculated using the band area for CO₂ measured during a complete and total photocombustion of 400 ppm of MeOH under high irradiation intensity (I₀=100%), which corresponds to the full capacity of the lamp. The photocombustion is then 100 % selective (CO₂ production) and the observed CO₂-band area corresponds to ~400 ppm of CO₂. This result has been used for estimating CO₂ concentration during the photooxidation of MeOH under different conditions. The CO₂-selectivity has been calculated as follows:

$$\text{CO}_2\text{-selectivity(\%)} = (n_{\text{CO}_2}) / (n_{\text{MeOH-converted}}) * 100$$

with:

n_{CO₂}= amount of CO₂ produced in mole.

n_{MeOH-converted}= amount of methanol converted in mole.

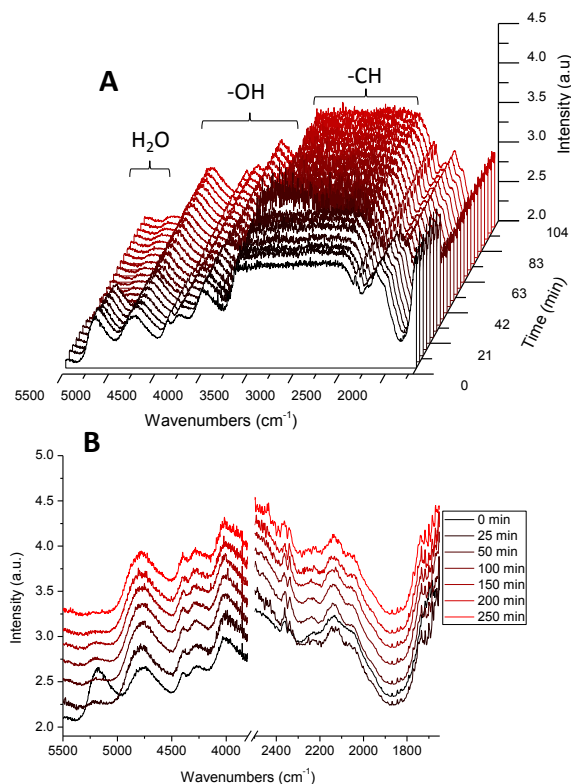


Fig.9 Evolution of the IR spectra of TiO₂/Luffa surface during methanol photooxidation under operando conditions. (Flow= 25 cm³/min, MeOH/O₂/Ar 400ppm/20%/79.99%, I₀=25% ~2.5 mW/cm² at 366nm).

The methanol photodegradation rate (V_{MeOH}) has also been calculated. It corresponds to the amount of methanol converted (n_{MeOH}) per second per gram of photocatalyst (g_{cat}). V_{MeOH} has been calculated with the following formula:

$$V_{\text{MeOH}} = [n_{\text{MeOH-converted}} \text{ (mmol)}] / [m_{\text{cat}} \text{ (g)} \times \text{time (s)}] \text{ (mmol/s/g}_{\text{cat}})$$

Due to the limitation of the irradiation on the external surface of TiO₂/Luffa pellet, the V_{MeOH} calculated are limit values.

The influence of methanol concentration has also been studied. The results are reported in Fig. 10 and shortlisted in Table 1. The

new bands that appear during the photooxidation are assigned to CO₂ (2400-2200 cm⁻¹) and -C=O of carbonyl species (1820-1670 cm⁻¹). As reported in previous works [32,34] an increase of concentration leads to a decrease of the CO₂-selectivity of the reaction. It is important to note that the CO₂-selectivity of the reaction increases the V_{MeOH} of the photodegradation reaction. This result could be assigned to the interaction of methanol in the gas phase with the active species adsorbed/formed on the photocatalyst surface.

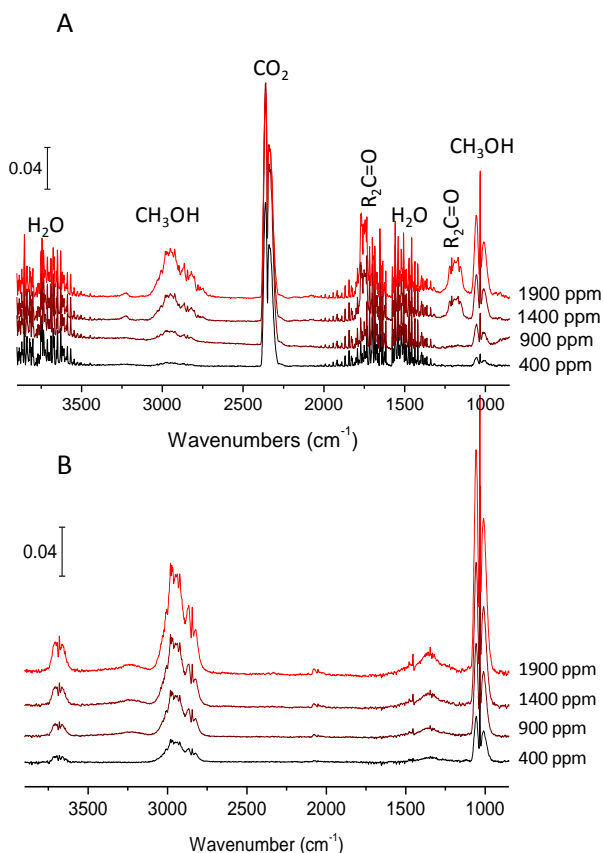


Fig.10 A) Evolution of the IR spectra of the gas phase during the photooxidation of methanol at different concentrations on TiO₂/Luffa composite. (Flow= 25cm³/min, I₀=25%). B) IR spectra of the gas phase before UV-irradiation of TiO₂/Luffa composite pellet, at different methanol concentrations.

Table 1 Reactivity, selectivity and rate of methanol photooxidation reactions under polychromatic irradiation for different methanol concentrations using TiO₂/Luffa composite as photocatalysts (Flow= 25 cm³/min, I₀=25%, m_{pellet}=90 mg → m_{TiO₂}~ 3mg).(*) Values founded using TiO₂-P25 as photocatalyst (m_{cat}=20 mg) in the same conditions.

[MeOH] (ppm)	Conversion (%)	CO ₂ -selectivity (%)	V _{MeOH} (mmol/s/g _{cat})
400	73.5 (100*)	100 (100*)	0.78 (0.2*)
900	73.6 (97*)	63.0 (90*)	1.75 (0.45*)
1400	66.0 (90*)	40.4(85*)	2.46 (0.65*)
1900	56.6 (85*)	26.0 (70*)	2.48 (0.83*)

A self supported TiO₂-P25 has been used as reference. Contrarily to V_{MeOH} which takes into account the weight of photocatalyst used, methanol conversion and CO₂-selectivity values could not be compared directly in the case of TiO₂/Luffa and TiO₂-P25 (Table 1) due to the different content (or amount) of TiO₂ used.

In the case of TiO₂/Luffa composite, the amount of TiO₂ is ~3mg (the weight of the TiO₂/Luffa pellet, ~90mg with TiO₂ content ~4%) while 20 mg of pure TiO₂-P25 has been used to prepare the pellet. Therefore, the comparison of the photocatalytic activity of TiO₂/Luffa with that of TiO₂-P25 only aims at having an idea about the activity of the composite. This comparison could not be quantitative due to the different nature of the two photocatalysts (e.g the internal shading effect in TiO₂/Luffa pellet is much higher than in TiO₂-P25 pellet).

A high activity is observed with TiO₂ present on the TiO₂/Luffa composite, with V_{MeOH} values higher than 2.5 mmol/s/g_{cat}. It is ~0.78 mmol/s/g_{cat} for a total methanol mineralisation (100% selectivity). The increase of the lamp intensity increases methanol conversion and CO₂-selectivity of the photooxidation reaction. The results are presented in table S-2 in SI. When the intensity of the lamp capacity is higher than 25% (which correspond to ~2.5 mW/cm² at 366nm), the conversion of 1900 ppm of methanol reaches its maximum (~74%) with total methanol mineralisation and V_{MeOH}~3.8 mmol/s/g_{cat}. In comparison, V_{MeOH} was 3 to 4 times higher on TiO₂/Luffa composite than on TiO₂-P25 in the same reaction conditions (Table 1). These high values could be assigned to the high TiO₂ dispersion and to the high surface area of TiO₂ on Luffa fibers, which increase the diffusion of methanol and the accessibility of active sites (S_{BET}(TiO₂ in TiO₂/Luffa composite)/ S_{BET}(TiO₂-P25)~7).

4. Conclusion

TiO₂ nanoparticles were successfully immobilized on a support of natural Luffa fibers by hydrothermal sol gel treatment. The net microstructures and hydroxyl groups of Luffa fibers provided a uniform dispersion of TiO₂ nanoparticles and a strong and complete recovery of the surface. The resulting TiO₂/Luffa composites showed high stability and efficiency in the photodegradation of methanol, model for VOCs in air. They also exhibited efficient removal of methylene blue from water. The photodegradation rate of methanol (V_{MeOH} in mmol/s/g_{cat}) on the new elaborated TiO₂/Luffa composite was 3 to 4 times higher than that on self supported TiO₂-P25 used as reference. These results could be explained by the high and uniform dispersion (high specific area) of TiO₂ supported on the Luffa support. This work showed that Luffa fibers are an ideal biosupport for photocatalytic applications of TiO₂. The non compact form, tridimensional structure, mechanical and chemical stability and low price of the newly elaborated composites make them very promising as green photocatalysts for air and/or water purification.

Associated content

The supporting information file contains:

- 1 scheme for the sandwich reactor-IR cell modified for UV catalysis study.
- 2 tables describing the different characteristics of the photocatalysts used in this work and their photocatalytic activity under different light intensities.
- Additional information related to the synthesis procedure (Figs. S.1 and S.2) and the capacity of the composites for the removal

and degradation of methylene blue.

Notes and references

- ^aLaboratoire Catalyse et Spectrochimie, ENSICAEN, Université de Caen, CNRS, 6, boulevard du Maréchal Juin, 14050 Caen, France. E-mail: mohamad.elroz@ensicaen.fr. Fax :0033 2 3145 2822, Tel : 0033 2 3145 2810,
- ^bLaboratoire de Matériaux, Catalyse, Environnement et Méthodes Analytiques, Université Libanaise, Rafik Hariri campus, Beyrouth-Hadath, Lebanon.
- ^cSchool of Mechanical and Materials Engineering Washington State University Pullman, WA Pullman, WA, USA 99164-2920, 5093394232.
- 1 L. Reijnders, *J. Hazard. Mater.* 2008, **152**, 440.
 - 2 M. Tashibi, C.R. Ngah, N. Aziz, A. Mansor, A.Z. Abdullah, L.K. Teong, A.R. Mohamed, 2007, **46**, 9006.
 - 3 J. Fernandez, J. Kiwi, J. Baeza, J. Freer, C. Lizama, H.D. Mansilla, *Appl. Catal. B* 2004, **48**, 205.
 - 4 J.C. Lee, M.S. Kim, B.W. Kim, *Water Res.* 2002, **36**, 1776.
 - 5 M.D. Nikolaki, D. Malamis, S.G. Pouloupoulos, C.J. Philippopoulos, *J. Hazard. Mater.* 2006, **137**, 1189.
 - 6 S. Horikoshi, N. Watanabe, H. Onishi, H. Hikada, N. Serpone, *Appl. Catal. B* 2002, **37**, 117.
 - 7 M.K. Aminian, N. Taghavinia, A. Irajizad, S.M. J. Mahdavi, *Phys. Chem. C* 2007, **111**, 9794.
 - 8 I.N. Martyanov, N.J. Klabunde, *J. Catal.* 2004, **225**, 408.
 - 9 M.G. Antoniou, D.D. Dionysiou, *Catal. Today* 2007, **124**, 215.
 - 10 Y. Xu, C.H. Langford, *J. Phys. Chem. B* 1997, **101**, 3115.
 - 11 F. Li, S. Sun, Y. Jiang, M. Xia, M. Sun, B. Xue, *J. Hazard. Mater.* 2008, **152**, 1037.
 - 12 S.N. Hosseini, S.M. Borghei, M. Vossoughi, N. Taghavinia, *Appl. Catal. B* 2007, **74**, 53.
 - 13 S.K. Kansal, M. Singh, D. Sud, *J. Hazard. Mater.* 2008, **153**, 412.
 - 14 T.H. Xie, J. Lin, *J. Phys. Chem. C* 2007, **111**, 9968.
 - 15 J. Shang, W. Li, Y. Zhu, *Mol. Catal. A* 2003, **202**, 187.
 - 16 N. Kieda, T. Tokuhisa, *J. Ceram. Soc. Jpn.* 2006, **114**, 42.
 - 17 H. Chen, S.W. Lee, T.H. Kim, B.Y. Hur, *J. Eur. Ceram. Soc.* 2006, **26**, 2231.
 - 18 I.R. Bellobono, R. Barni, F. Gianturco, *J. Membr. Sci.* 1995, **102**, 139.
 - 19 P. Lei, F. Wang, X. Gao, Y. Dinga, S. Zhang, J. Zhao, S. Liu, M. Yang, *J. Hazard. Mater.* 2012, **227**, 185.
 - 20 D.E. Tsydenov, V.N. Parmon, A.V. Vorontsov, *Intern. J. Hydrogen Energ.* 2012, **37**, 11046.
 - 21 Z. Liuxue, W. Xiulian, L. Peng, S. Zhixing, *Surf. Coat. Technol.* 2007, **201**, 7607.
 - 22 B. Tryba, *J. Hazard. Mater.* 2008, **151**, 623.
 - 23 T. Pekdemir, B. Keskinler, E. Yildiz, G.J. Akay, *Chem. Technol. Biotechnol.* 2003, **78**, 773.
 - 24 E. Ghadiri, N. Taghavinia, S. Zakeeridin, M. Gatzel, J. Moser, *Nano Let.* 2010, **10**, 1632.
 - 25 J.-P. Chen, S.-C. Yu, B.R.-S. Hsu, S.-H. Fu, H.-S. Liu, *Biotechnol. Prog.* 2003, **19**, 522.
 - 26 C.A. Boynard, S.N. Monteiro, J.R.M. d'Almeida, *J. Appl. Polym. Sci.* 2002, **87**, 1927.
 - 27 A. Zampieri, G.T.P. Mabande, T. Selvam, W. Schwieger, A. Rudolph, R. Hermann, H. Sieber, P. Greil *Mat. Sci. and Eng. C* 2006, **26**, 130.
 - 28 T. Lesage, C. Verrier, P. Bazin, J. Saussey, M. Daturi, *Phys. Chem. Chem. Phys.* 2003, **5**, 4435.
 - 29 M. El-Roz, M. Kus, P. Cool, F. Thibault- *J. Phys. Chem. C*, 2012, **116**, 13252.
 - 30 F. Thibault-Starzyk, A. Vimont, J.P. Gilson, *Catal. Today* 2001, **70**, 227.
 - 31 M. El-Roz, P. Bazin, F. Thibault-Starzyk, *Catal. Today*, 2012, **DOI: 10.1016/j.cattod.201208.023**.
 - 32 A. Houas, H. Lachheb, M. Ksibi, E. Elaloui, C. Guillard, J.M. Herrmann, *Appl. Catal. B* 2001, **31**, 145.